Karlsruhe Institute of Technology

Validation of the swelling formalism via evaluation of bending moments from literature

- Comparison of theoretical predictions and measurements

K. G. Schell, T. Fett, C. Bucharsky

KIT SCIENTIFIC WORKING PAPERS 187

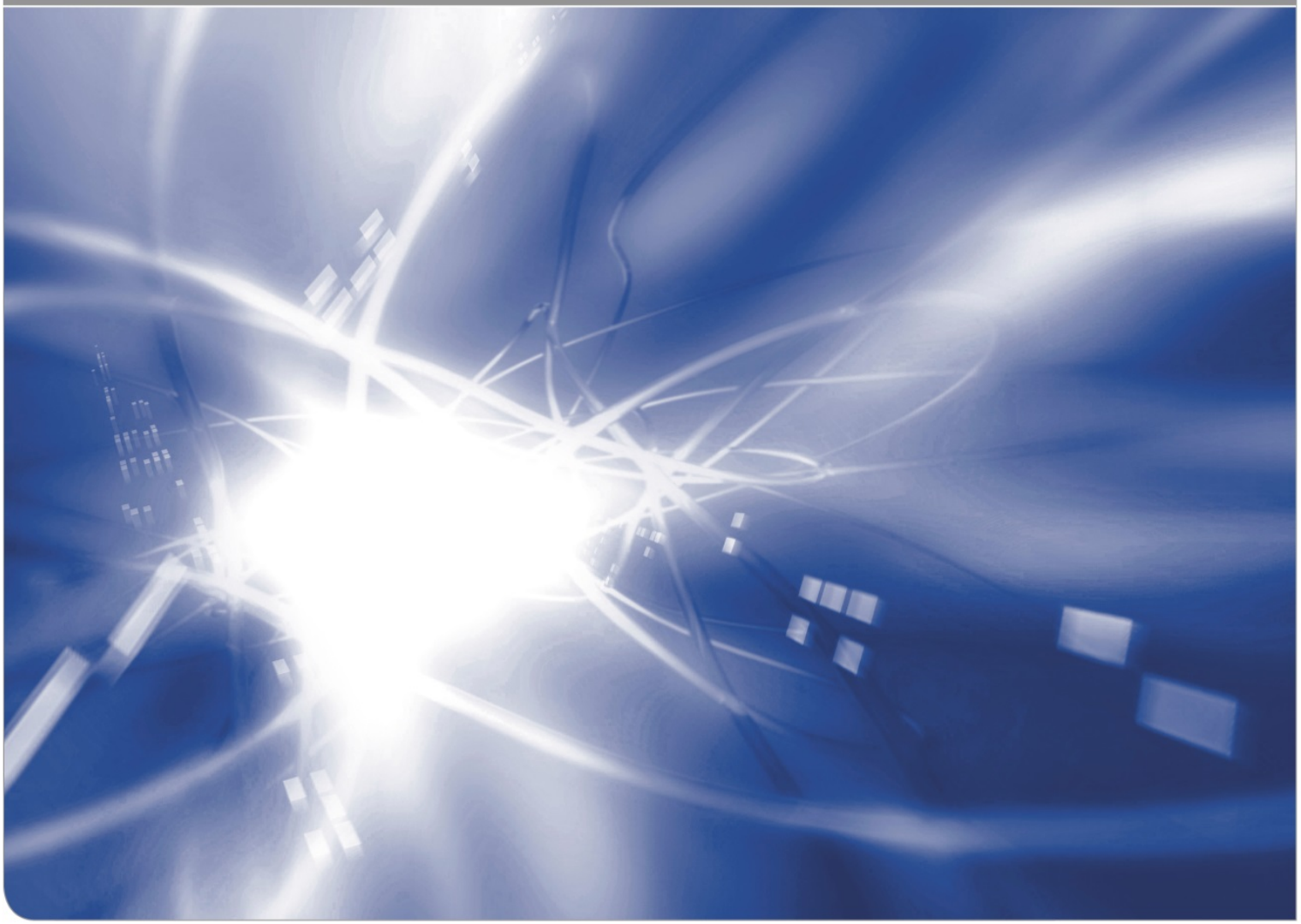

Institute for Applied Materials

Impressum

Karlsruher Institut für Technologie (KIT)
www.kit.edu

2022

ISSN: 2194-1629

Abstract

The volume of silica expands by the hydroxyl generation when silica surfaces react with water. These volume strains are proportional to the mass concentration of the hydroxyl. They were measured by Wiederhorn et al. by evaluating the curvature of disks undergoing this reaction on only one side. The obtained bending moments were found to be proportional to square-root of heat-treatment time.

In the present considerations we pay particular attention to global bending moments caused by swelling, which, in contrast to local swelling stresses, do not require assumptions about the type of stress distribution.

It can be stated that

- The bending moments from disk curvature and hydroxyl measurements via the IR-evaluation procedure by Libowitzky and Rossman are in excellent agreement.
- Predictions of moments M based on diffusivities and surface water concentrations by Helmich and Rauch also show good agreement with correlation coefficients $R^2>0.95$. Consequently, we can sufficiently write: $M_{\text{predict}} = M_{\text{measured}}$.

Contents

1 Basic results

When silica reacts with water, the volume expands by the hydroxyl generation. The volume strain reads in terms of hydroxyl mass concentration *S* [1,2]:

$$\varepsilon_v = \tfrac{18}{17}(1+\chi)\frac{S}{2} = \kappa \times S \ , \ \kappa = 0.97 \ \ [0.92,1.02] \qquad (1)$$

In eq.(1) the numbers in brackets represent the 95% confidence interval. The volume increase ε_v is plotted in Fig. 1 versus the hydroxyl concentration *S* for the data in [2]. The straight line represents the coefficient κ=0.97 according to (1). The good agreement with all the data is evident.

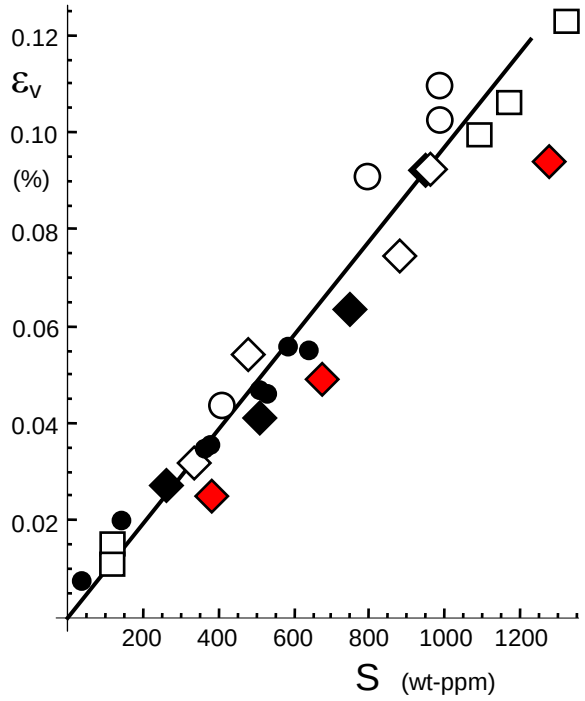

Fig. 1 Expansion vs. hydroxyl concentration *S*, from [1, 2], different symbols represent different authors and fictive temperatures. Circles: Shelby [3], Squares: Brückner [4, 5], Diamond squares: Shackelford [6].

The effect of the water-silica reaction is the generation of *swelling strains*. *Swelling stresses* are a consequence of the mechanical boundary conditions. A volume element in a thick plate that undergoes swelling cannot freely expand. If the diffusion zone is small compared to the component dimensions, expansion is completely prevented in the plane of the surface and can only take place normal to the surface plane.

At a free surface, the stress state is *plane stress* and, consequently, also stresses caused by swelling are equi-biaxial (σ_x=0)

$$\sigma_{sw,y} = \sigma_{sw,z} = -\frac{\varepsilon_v E}{3(1-\nu)} \tag{2}$$

In (2) E is Young's modulus and ν is Poisson's ratio. Consequently, the hydrostatic stress term reads

$$\sigma_{sw,h} = \tfrac{1}{3}(\sigma_{sw,y} + \sigma_{sw,z}) = -\frac{2\,\kappa E}{9(1-\nu)} S = -18.7\ \text{GPa} \times S \tag{3}$$

2 Swelling from measurement of disk curvature

Swelling stresses were derived in [10] by measuring the change of the curvature of silica disks after hot-water soaking. At the heart of this study is an experiment in which water is diffused into one side of thin vitreous silica disks. This technique has been used earlier to determine the volume change caused by the penetration of water into silica coatings on silicon wafers [7]. The consequent volume expansion at the glass surface results in a bending of the disks, which are no longer flat after exposure, but concave-shaped [7]. By measuring the radius of curvature at the surfaces of the curved disks and by understanding the mechanism of water migration, the surface stress can be calculated. The technique can also be used to calculate the diffusivity of water in silica glass.

A plate is considered with all dimensions very much larger than the water diffusion zone b which is given by

$$b = \sqrt{Dt} \tag{4}$$

The bending moment caused by a thin swelling layer is then given as

$$M_b = \int_0^\infty \sigma(z)(\tfrac{1}{2}W - z)\,dz \underset{z<<W}{=} \frac{W}{2}\int_0^\infty \sigma(z)\,dz \tag{5}$$

Figure 2 shows the measured moments plotted versus square root of time. The relatively large scatter in Fig. 2a is mainly caused by the deviations of the test temperatures from the nominal temperature T=200°C.

The measured change of the bending moment is plotted in Fig. 2a for measurements at about 200°C and in Fig. 2b for 90°C. The solid symbols in Fig. 2b represent tests carried out in liquid water. Within the 95% confidence lines, there is no significant difference visible between vapour and water.

The regression data are compiled in Table 1 for the representation

$$-M_b = A\sqrt{t} \tag{6}$$

In column 2 the coefficient for eq.(6) is given together with the 90%-Confidence Interval (column3). Column 4 contains the correlation coefficient R^2 as a measure of the quality of linear regression. It indicates how well the independent variables are able to explain the variance of the dependent ones. The R^2 is always between 0 (unusable model) and 1 (perfect model fit). It is easily interpreted as the proportion of the variance of the dependent variable (explained variable) that can be explained by the independent variables (explanatory variables).

Temperature	A (Nm/(m√h))	90%CI	R^2
200°C	4.08×10^{-3}	[0.00337, 0.00478]	0.912
90°C	1.303×10^{-4}	[1.11×10^{-4}, 1.41×10^{-4}]	0.910

Table 1: Regression data for the measured bending moments in form of eq.(6).

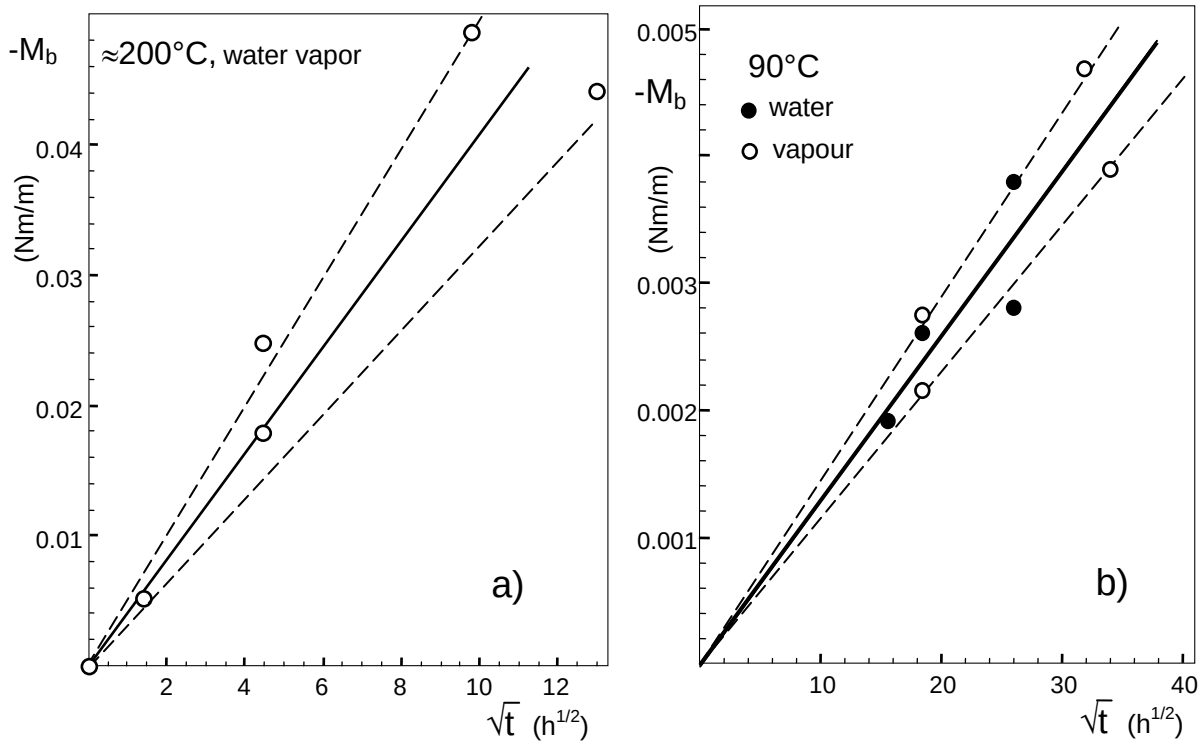

Fig. 2 Measured bending moments (via disk curvature) versus time (circles) for elevated temperatures. Zouine *et al.* [8].

3 Total moment compared to predictions from IR-measurements

In a second attempt the total water uptake m_{Cw} was used as measured by IR as well as the *S*/*C* ratio also obtained from IR using the evaluation procedure by Libowitzky and Rossman [9]. The IR-evaluation in transmission was performed in [10] on the "free"

OH stretch at ≈3680 cm^{-1} and the hydrogen-bonded OH stretch at ≈3610 cm^{-1}, together with the bound and free water bands at ≈3400 $cm^{-1}$and ≈3200 cm^{-1} [9].
As shown in [10] it holds for the generated bending moment expressed in terms of the hydroxyl concentration S

$$M_b = -\kappa \frac{W}{2} \frac{E}{3(1-\nu)} \cdot \underbrace{\int_0^\infty S(z)dz}_{m_S} \tag{7}$$

where m_S is the uptake of the hydroxyl water from one side.
Curvature measurements on water-vapor soaked disks of the silica GE-124 (a type-I glass) were carried out in [10]. By measuring the radius of curvature at the surfaces of the curved disks, the change of bending moments can be concluded. For the prediction of bending moments from the IR-measurements, we use the results for 196°C. At this temperature, bending moments after 20h vapour soaking can be compared with the IR-result for 18h vapour soaking after a small correction from 18h to 20h (see Fig 3a). After the 20h treatment, the thickness of the diffusion zone is slightly higher than for 18h due to eq.(4). Also the surface concentration increases slightly. This is illustrated in Fig. 3a by using the measurements of Helmich and Rauch [11]. Both corrections together result in the water uptake compiled in Column 4 of Table 2.

Temperature/ Exposure Time	Water content from IR [10] $m_{Cw,200°C}$	Predicted Moment from IR via eq.(7)	Time correction to t=20h via $m_{Cw} \propto C_w\sqrt{t}$	Measurement [10]
196°C/18h	4.7 nm	-0.0145 Nm/m		
196°C/20h			-0.0157 Nm/m	-0.0173 Nm/m
90°C/1008h	2.2 nm	-0.0047 Nm/m		-0.00469 Nm/m

Table 2: Predicted and measured bending moments.

4 Total moment predicted via diffusivity and water concentration

The experimental results on equilibrium ratios from literature were expressed in [10] for the temperature range of 90°C≤T≤350°C by the empirical relation

$$k = \frac{S}{C} = A \exp\left(-\frac{Q}{RT}\right) \tag{8}$$

(A=32.3 and Q=10.75 kJ/mol). The hydroxyl concentration S results from the total water concentration C_w in molar units

$$S = \frac{C_w}{\left(\frac{1}{2} + \frac{1}{k}\right)} \tag{9}$$

and in *mass units* considering the different mole masses of water and hydroxyl

$$S = \frac{17}{18}\frac{C_w}{\left(\frac{1}{2} + \frac{1}{k}\right)} \tag{9a}$$

Figure 4a shows the surface concentration of water depending on temperature θ. The results by Zouine et al. [8] in liquid water are given by the open circles. Data of Helmich and Rauch [11] for water vapour under saturation pressure are shown by the coloured symbols for different temperatures. From these data, the hydroxyl concentration can be determined by eqs.(8) and (9a) The hydroxyl concentrations are plotted in Fig. 4b for the case that the reaction between water and silica is in equilibrium even for the short time of 5h.

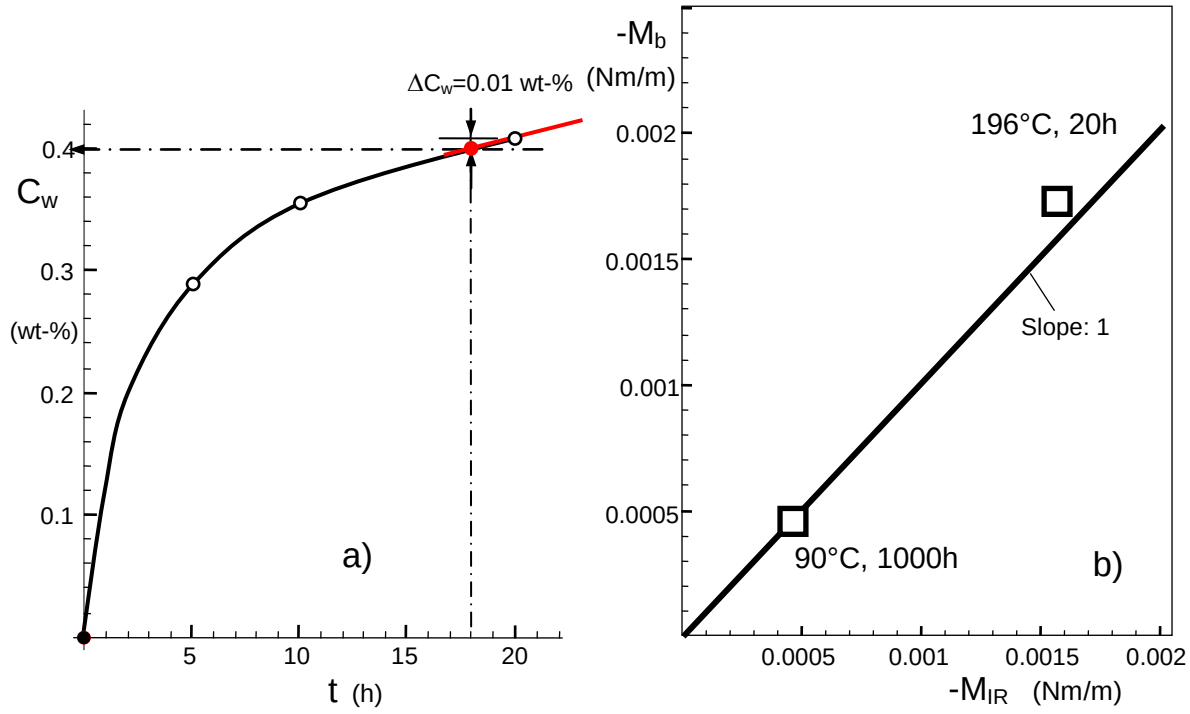

Fig. 3 a) Evaluation of surface water concentration C_w for $t = 18$h; a) transformation of water concentration from 20h (bending) to 18h (IR), b) measured bending moment vs. the moment predicted from IR measurements.

Figure 5 compiles data of the effective diffusivity as function of the temperature. The red circles show data by Helmich and Rauch [11], measured on specimens heat-treated in water vapour under saturation pressure. The red squares also indicate data from Wiederhorn et al. [10] heat treatment in saturation vapour. In this case the diffusivity

was obtained assuming that the stresses would be erfc-shaped distributed. Finally, the black circles are results by Zouine et al. [8] on liquid-water soaked specimens.

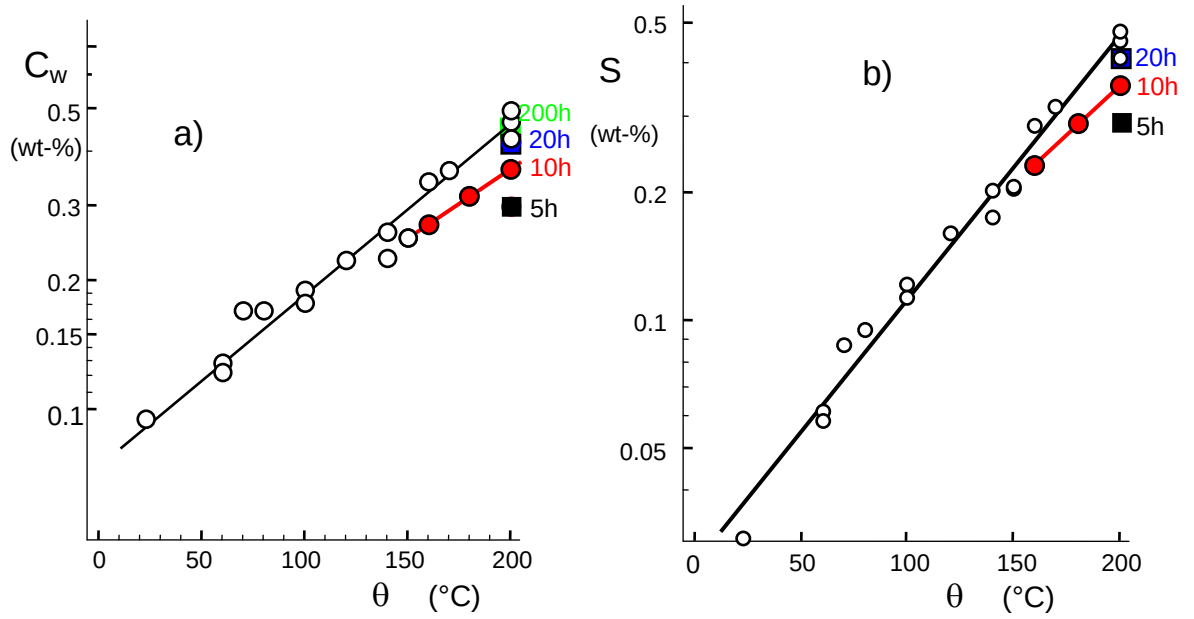

Fig. 4 a) Solubility of water at silica surfaces under saturation pressure by Zouine et al. [8] (open circles) and Helmich and Rauch [11] (red circles and squares); b) hydroxyl water species (same symbols as in part a)).

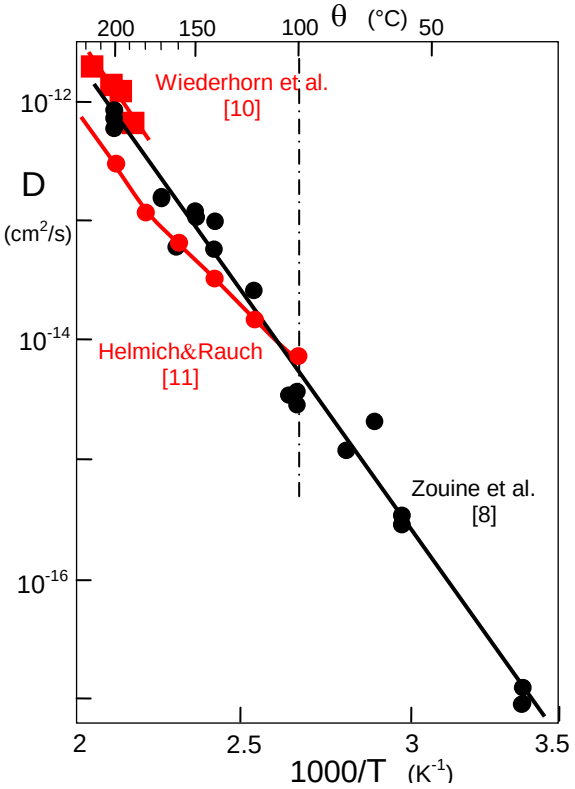

Fig. 5 Diffusivities; black circles: results for silica soaked in *liquid water* under saturation pressure by Zouine et al. [8], red symbols: after soaking in *water vapour* of saturation pressure.

All predictions are compiled in Column 8 of Table 3. Figure 6 shows the measured vs. the predicted moments. The black straight-line represents the slopes of Table 4 and the red line is the theoretically expected one.

The deviating data point in parentheses suggests the existence of an outlier. To show this, this point is omitted in Fig. 6b and the calculation is repeated. There is a large improvement in the more robust dependency. The width of the 90% confidence interval is practically halved. The improvement in the correlation coefficient R^2, expressed by the deviation from the ideal coefficient $R^2 = 1$, $1\text{-}R^2$, is about a factor of 10.

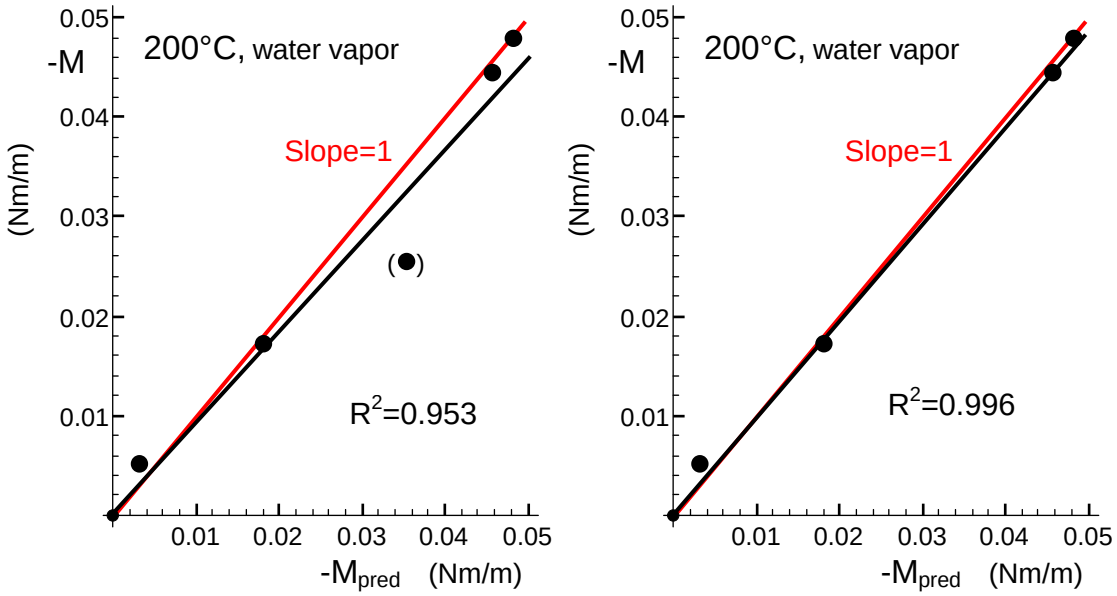

Fig. 6 Measured total bending moment M compared with predictions M_{pred} based on the data by Helmich and Rauch [11], possible outlier indicated by data point in parentheses.

Temperature/ Time	C_{w0} [11] (wt-%)	D [11] (cm^2/s)	$b=\sqrt{Dt}$ (µm)	S (wt-%)	m_S (nm)	M [10] (Nm/m)	M_{pred} (Nm/m)
196°C/2h	0.20	2.3×10^{-13}	0.407	0.194	0.915	0.0051	0.0030
196°C/20h	0.41	2.3×10^{-13}	1.29	0.39	5.76	0.0173	0.0178
216°C/20h	0.47	6×10^{-13}	2.08	0.50	11.42	0.0255	0.0371
201°C/96h	0.43	3×10^{-13}	3.22	0.416	15.1	0.048	0.0482
188°C/168h	0.425	1.7×10^{-13}	3.21	0.395	13.6	0.0447	0.0480

Table 3: Water concentration at the surface under saturation pressure based on measurements by Helmich and Rauch [11].

Evaluation	Slope	90% CI	R^2	$1\text{-}R^2$
Outlier included	0.904	[0.795, 1.013]	0.953	0.047
Outlier excluded	0.964	[0.916, 1.012]	0.996	0.004

Table 4: Test on outlier in Fig. 6a.

The outlier can be ignored in the following, but has to be checked afterwards for a possible special effect. The significantly higher measuring temperature of 216°C and the change of water coverage on the glass surface at about 200°C will play a role in such a consideration [12]. The same may hold for the mass transfer coefficient [13, 14].

Main Conclusions*:*

- The measured bending moments are proportional to square-root of heat-treatment time.
- The moments from disk curvature and hydroxyl measurements via the IR-evaluation by Libowitzky and Rossman [9] are in excellent agreement, Fig. 3b.
- Predictions of moments M based on diffusivities and surface water concentrations [11] also show agreement with correlation coefficients R^2>0.95. Consequently we can sufficiently write $M = M_{\text{pred}}$.
- As a global quantity, the moment of course says nothing about how the related tensile stresses stresses leading to it are distributed across the water zone.

References

1 S. M. Wiederhorn, M. J. Hoffmann, T. Fett, Swelling strains from density measurements, Scientific Working Papers **38**, 2015, KIT Scientific Publishing, Karlsruhe.

2 T. Fett, K.G. Schell, S.M. Wiederhorn, Molar volume of SiOH estimated from swelling strains, International Journal of Applied Glass Science, **11** (2020), 608-611.

3 Shelby, J.E., "Density of vitreous silica," J. Non-Cryst. **349** (2004), 331-336.

4 Brückner, R., "The structure-modifying influence of the hydroxyl content of vitreous silicas," Glastech. Ber. **43** (1970), 8-12.

5 Brückner, R., "Metastable equilibrium density of hydroxyl-free synthetic vitreous silica," J. Non-Cryst. Solids, **5** (1971), 281-5

6 Shackelford, J.F., Masaryk, J.S., Fulrath, R.M., "Water Content, Fictive Temperature and Density Relations for Fused Silica," J. Am. Ceram. Soc. **53** (1970), 417.

7 P.A. Flinn, Principles and Applications of Wafer Curvature Techniques for Stress Measurements in Thin Films, *Mat. Res. Soc. Symp. Proc.* **130** (1989), 41-51.

8 A. Zouine, O. Dersch, G. Walter and F. Rauch, Diffusivity and solubility of water in silica glass in the temperature range 23-200°C, *Phys. Chem. Glass: Eur. J. Glass Sci and Tech. Pt. B*, **48** [2] (2007), 85-91.

9 E. Libowitzky and G.R. Rossman, "An IR absorption calibration for water in minerals," *Amer. Mineroalogist*,**82**, 1111-1115 (1997).

10 S. M. Wiederhorn, F. Yi, D. LaVan, T. Fett, M.J. Hoffmann, Volume Expansion caused by Water Penetration into Silica Glass, J. Am. Ceram. Soc. **98** (2015), 78-87.

11 M. Helmich and F. Rauch, On the mechanism of diffusion of water in silica glass, *Glastech. Ber.* **66** [8] (1993), 195-200.

12 L.T. Zhuravlev, The surface chemistry of amorphous silica. Zhuravlev model, *Colloids and Surfaces, A: Physicochemical and Engineering Aspects* **173**(2000), 1-38.

13 G. Schell, T. Fett, Mass transfer coefficients for water at silica surfaces - Additional results, **73**, 2017, ISSN: 2194-1629, Karlsruhe, KIT.

14 T. Fett, G. Schell, Water concentration and swelling stresses at silica surfaces derived from literature data - Estimation of mass-transfer coefficients, **94**, 2018, ISSN: 2194-1629, Karlsruhe, KIT.

KIT Scientific Working Papers
ISSN 2194-1629

www.kit.edu